# Preparation of carbon nanofibers/tubes using waste tyres pyrolysis oil and coal fly ash derived catalyst

KHAVHARENDWE. M. RAMBAU[1,2], NICHOLAS M. MUSYOKA[1*], NCHOLU MANYALA[2*], JIANWEI REN[1], HENRIETTA W. LANGMI[1], MKHULU K. MATHE[1]

[1]*Energy Centre, Council for Scientific and Industrial Research (CSIR), Pretoria, South Africa.*

[2]*Department of Physics, Institute of Applied Materials, SARCHI Chair in Carbon Technology and Materials, University of Pretoria, South Africa.*

## Abstract

In this study, two waste materials namely; coal fly ash (CFA) and waste tyres pyrolysis oil, were successfuly utilised in the synthesis of carbon nanofibers/tubes (CNF/Ts). In addition, Fe-rich CFA magnetic fraction (Mag-CFA) and ethylene gas were also used for comparison purposes. The carbons obtained from CFA were found to be anchored on the surface of the cenosphere and consisted of both CNTs and CNFs whereas those obtained from Mag-CFA consisted of only multi-walled carbon nanotubes (MWCNTs). The study further showed that the type of carbon precursor and support material played an important role in determining the nanocarbon growth mechanism. The findings from this research have demonstrated that it is possible to utilize waste tyres pyrolysis oil vapour as a substitute for some expensive commercial carbonaceous gases.

---

*Address correspondence to Nicholas M. Musyoka (Energy Centre, Council for Scientific and Industrial Research (CSIR), Pretoria, South Africa) E-mail:- nmusyoka@csir.co.za or Ncholu Manyala (Department of Physics, Institute of Applied Materials, SARCHI Chair in Carbon Technology and Materials, University of Pretoria, South Africa) E-mail:- ncholu.manyala@up.ac.za.

**Keywords:**. Carbon nanofibers/tubes; multiwalled carbon nanotubes; waste tyres; pyrolysis oil vapor

## Introduction

Carbon nanomaterials (CNMs) are amongst the most well-known and studied nanomaterials with many industrial applications and are known to exist in different forms such as; 0D (fullerenes), 1D (carbon nanotube/fibers) and 2D (graphene).[1-5] The diameters of these CNTs and CNFs typically range from 1 nm to about 100 nm and their lengths can vary from 10 nm to a few centimetres. CNTs are cylindrical graphene sheets and can be classified in three forms; single walled (SWCNTs), double-walled (DWCNTs), or multi-walled (MWCNTs).[1,6-8] On the other hand, the graphene layers of the cylindrical CNFs nanostructures are stacked as cones, cups or plates.[9,10] Importantly, CNFs are reportedly wider (> 100 nm) in appearance than CNTs (mostly with internal diameters of < 50 nm). CNT/Fs are conventionally produced from the catalytic decomposition of hydrocarbon gases over selected metal nanoparticles such as copper, iron, nickel, among others that are often dispersed on the substrate.[10-12] Examples of powder support substrates which are mainly used are; $Al_2O_3$, $SiO_2$, $TiO_2$ and MgO.[13,14] In most cases, the above synthesis procedure often utilizes commercially available support materials and the carbon precursors such as ethylene, benzene and acetylene which are quite expensive. This challenge has led the research community into a quest for finding cheap feedstocks to substitute the conventional way of synthesis.[13-18] There have been reports of synthesizing CNMs using raw materials such as lava, natural minerals and botanical hydrocarbons.[19] However, there is still a need to identify other low-cost feedstocks.

In this study, we report the use of coal fly ash (CFA) and its magnetic fraction as catalyst and support. CFA is a by-product of coal combustion process and contains significant amounts of silicon and aluminium oxides (both amorphous and crystalline) as well as other trace elements.[20-22] We further report on the use of waste tyres pyrolysis oil vapour as a carbon precursor. Pyrolysis oil is one of the key by-products obtained from thermal degradation of waste tyres in an oxygen free environment.[23,24] Even though there have been some reports on utilization of South African CFA as support material for CNMs growth, the obtained CNMs were CNFs and in small quantity. The results further showed that the presence of iron (in the form of an oxide) in the CFA was the catalyst that enhanced the growth of the obtained CNFs.[25] The group had also utilized commercially available acetylene as carbon precursor to generate CNFs. Other confirmations of CNMs grown using CFA were reported using Japanese CFA based on use of methane and ethanol as the carbon source to grow MWCNTs by thermal chemical vapour deposition (CVD) process.[26] There have been few reports of iron extraction from the CFA to establish if they could serve as valuable product in sensors, catalysts and environmental remediation but no reports for their use in the production of carbon CNMs. [27,28] Since the iron oxides in the CFA play an important role in the growth of CNMs, our research aimed at isolating iron oxides (or the magnetic component) of the CFA in order to synthesise better quality CNT/CNFs. Additionally, the utilization of waste tyres pyrolysis oil vapour as carbon precursor will play an important role in replacing the expensive carbon precursors.

## Experimental

### *Materials*

Sulphuric acid ($H_2SO_4$, 37%), furfuryl alcohol ($C_5H_6O_2$, 98%) and ethanol ($C_2H_6O$, 99.5%) were purchased from Associated Chemical Enterprise (South Africa). Argon (Ar), hydrogen ($H_2$) and ethylene ($C_2H_4$) gases were supplied by Afrox. Coal fly ash was supplied by a South African power station.

***Synthesis of carbon nanomaterials on coal fly ash and its magnetic fraction***

Acid digestion process was conducted in order to separate the magnetic materials from the coal fly ash (CFA). This was done by mixing the CFA with $H_2SO_4$ at a ratio of 1:2 and the mixture was heated to 200 °C for 4 hours. The mixture was then diluted with deionized water and the magnetic fragments were collected using a magnetic rod and then dried in the oven at 90 °C for 12 hours. The CFA and its magnetic fraction were placed separately in a ceramic boat and thereafter transferred to the tube furnace that had been connected to gas supplies for the chemical vapour deposition (CVD) process. The temperature of the furnace was set to 700 °C with a ramping rate of 5 °C/min under argon flow at a rate of 500 mL/min. At this temperature, a mixture of hydrogen and argon was allowed to flow into the tube furnace (at a ratio of 1:5). Hydrogen serves to reduce the iron oxides whereas its mixture with argon is only for safety reasons. This gas mixture was allowed to flow through for 1 hour and thereafter the temperature of the furnace was decreased to 650 °C. Thereafter, a carbon precursor (either ethylene or pyrolysis oil vapour) was then introduced at a flow rate of 250 mL/min. In the case of pyrolysis oil gas, a flow through valve that enabled bubbling of argon through the pyrolysis oil was opened. The temperature in the furnace was maintained at 650 °C for an additional 1 hour while the Ar/$H_2$/carbonaceous gas flowed

through. The resulting CNMs grown on CFA were denoted as CFA-Cethy (using ethylene gas) and CFA-Cpy (using pyrolysis oil vapour). On the other hand, CNMs grown on the magnetic fraction were denoted as Mag-Cethy (ethylene synthesized) and Mag-Cpy (from pyrolysis oil vapour).

***Material Characterization***

The pyrolysis gas/vapour collected by bubbling argon through pyrolysis oil was sampled using Tedlar® gas bags and analysed on the thermal desorption Gas chromatography–mass spectrometry (GC-MS) and Gas Chromatography – Flame Ionization Detector (GC-FID) to determine the presence of Benzene, Toluene, Ethylbenzene and Xylene (BTEX). The morphology of the obtained carbonaceous materials was analysed using an Auriga Cobra Focused-Ion Beam Scanning Electron Microscope (FIB-SEM). SEM Energy Dispersive Spectroscopy (EDS) was used for elemental analysis of the as-received CFA and its magnetic fraction. X-ray diffraction (XRD) patterns were obtained using a PANalytical X'Pert Pro powder diffractometer with Pixcel detector using Ni-filtered Cu-Kα radiation (0.154 nm) in the range of $2\theta$ = 1–60°, and at a scanning rate of $0.1°s^{-1}$. The Raman analysis was performed using Jobin-Yvon T64000 Raman spectrometer. Transmission electron microscope (TEM) images of the carbon materials were obtained using a JEOL-JEM 2100 TEM model.

**Results and Discussion**

The resulting pyrolysis gas mixture was found to contain some of the carbonaceous fraction known to be present in the pyrolysis oil.[29] Some of the identified gases were; benzene, toluene, ethylbenzene, m/p-xylene and o-xylene (BTEX). This carbon-rich fraction was utilized as a precursor for the growth of the carbon nanomaterials. Table 1 gives an indication of the presence of Si, Al, Fe and other trace elements on both the as-received CFA and its magnetic fraction. These elements are the primary constituents which form the mineral composition of CFA.[25] After the isolation of the magnetic fraction, the weight percentage of the major elements (Si and Al) was noted to have decreased significantly, however, there was an increase in the Fe content. Most of the Fe in the CFA is reported to be present in the form of magnetite which is magnetic and hence its enrichment in the extracted sample.[28,30]

Coal fly ash is known to consist of various minerals that are present in their oxide form.[28] The most dominant minerals are; quartz, mullite, glassy aluminosilicates phases (composed of the non-crystalline materials) and Fe-rich minerals which are hematite and magnetite.[28-30] These minerals were also found to be present in the CFA magnetic fraction, as shown in the XRD patterns in Figure 1. The CNMs samples obtained from the as-received CFA and its magnetic extract were also found to contain mineral phases observed in ther parent materials (Figure 2 and 3). Previous work reported that the peaks appearing at $2\theta=25.5^{o}$ and $2\theta=43^{o}$ are due to the respective 002 and 100 plane of the graphitic structure of the CNMs.[31-34] The peak at $2\theta=44.06^{o}$ signifies the reduction of Fe oxide to pure iron metal whereas the peak at $2\theta=45.01^{o}$ is as a result of formation of iron carbide during the CVD process.[35-37] It was also noted that most of these peaks were overlapping with the peaks of mullite phase for all samples produced either using ethylene or pyrolysis oil vapour. To further confirm the presence of graphitic materials, these carbonaceous materials were analyzed using Raman Spectroscopy.

Figure 4a presents the SEM image of the as-received CFA and shows the its morphology. The observed cenospheres are known to consist of an amorphous glassy phase and is formed as a result of decomposition of minerals such as carbides, carbonates and sulphates which give off gaseous products. This process occurs during the heating and cooling stages in the pulverized coal boiler.[38-39,51] Figure 4b presents the SEM image of magnetic fraction extracted from CFA. The morphology consists of irregular shapes together with some spherical shapes that are from the as-received CFA. The morphological difference of CFA and Mag-CFA is attributed to the etching out of the soluble phases from the iron-rich mineral phases. Figure 4c depicts the carbon nanomaterials that were grown from CFA using ethylene as carbon precursor. According to the obtained results for CFA-Cethy, the grown CNMs consist of tubular or cylindrical materials with different diameters. The thicker (or larger diameter) materials were mostly randomly distributed whilst the thinner ones were mostly anchored on the surface of the cenospheres. The thicker cylinders had a diameter of around 100 nm whereas the thinner ones had an average diameter of 28 nm. These results are consistent with previous reports where CNMs were grown on Australian coal fly ash and showed the presence CNMs with different diameters and later confirmed with the TEM images to be CNFs and CNTs.[25] Figure 4d presents SEM image of CNMs grown on CFA using pyrolysis oil vapour as carbon precursor. The obtained CNMs were not as distinct as those grown using ethylene as carbon precursor and were mostly found to be anchored on the surface of the cenospheres. Figure 4e shows the SEM image of the CNMs grown on the extracted magnetic fraction using ethylene. The image depicts thin cylindrical structures that are clustered and forming ‘cobweb-like’ structures. These materials were dispersed throughout the support and had average dimeters of about 30 nm. Figure 4f shows the CNMs that were grown using pyrolysis oil vapour were not as prominently or thoroughly formed and were observed to have thin tubular structure but at relatively low quantity. As mentioned earlier, the pyrolysis oil vapour consists of various contents of hydrocarbons and they also vary in quantity. On the other hand, ethylene gas is rich in a single type carbon constituent and thus acts as the determining factor for the type and

quantity of the growth of the carbon nanomaterial. Conventionally, carbon nanomaterials are mostly grown using ethylene, benzene, xylene and methane as the carbon precursor and factors such as vapour pressure, temperature, gas flow rate and concentration of the carbon precursor affect the growth rate and/or the type of CNMs. [40-41,52]

Figure 5a and b presents TEM images of CNMs that were grown on CFA and Mag-CFA, respectively. By using their morphology as identification of the CNMs type, it was seen that the CNMs grown on the as-received CFA were mostly CNFs even though there were some trace CNTs masked by the CNFs, when images were taken in different sample regions. The nanocarbons were seen to be anchored on the surface of the cenospheres, as previously confirmed by SEM. The results correspond to what Hintsho et al had obtained. [26] The group had utilized South African coal fly ash as support and acetylene as carbon precursor to generate CNFs and also found that the resulting CNFs were anchored on cenospheres surface. The CNMs obtained from the Mag-CFA were multi-walled carbon Nanotubes (MWCNTs) as shown by Figure 5b. The TEM images show the MWCNTs having 14 walls on each side. The diameters of the tubes were in the range of 12-30 nm. The distance between the two inner walls was 8 nm. Figure 5c depicts the type of growth mechanism the CNFs embarked on. As seen on the image, there is a metal nanoparticle that is situated at the tip of the filament which indicates that there was a tip-growth mechanism as depicted by Figure 6a. This tip-growth phenomenon is due to the weak interaction between the metal catalyst and the support and occurs during the precipitation step where the carbon precipitates at the bottom of the metal which in turn dislocates the metal particle from the support and triggers the growth of the CNT/Fs.[45-47] Some few CNTs were also observed to contain a nanoparticle at their tips (Figure 5b) indicating some similarity in the growth mechanism. On the contrary, the CNT/Fs without the nanoparticle at their tips are expected to have followed the root-growth mechanism (where the catalyst particle is found at the bottom of

the tube).[10] The root-growth mechanism is favoured when the catalyst–support interaction is strong.[10] These results are consistent with previous reports.[25-26] The internal morphology of the CNFs is also depicted in the zoomed insert on Figure 5a and can be seen to depict herringbone morphology as elaborated in Figure 6b. In this morphology, the graphene layers are arranged in a fish-bone structure along the vertical axis of the carbon filament.[15,53]

The growth mechanism of CNMs is known to be exothermic in nature, therefore, there is a temperature gradient at the catalyst particle.[46,48] With the solubility of carbon on metal catalyst dependent on temperature, precipitation occurs at the colder zones of the metal catalyst and thus allowing the carbon filament to grow at the same diameter as the metal catalyst.[48-49] This suggests that obtaining a combination of CNFs and CNTs on the as-received coal fly ash was due to the different particle sizes of the metal catalyst. The isolation process through the magnetic extraction gave a selection of uniform particle distribution thus enabling MWCNTs to be obtained.[26, 46,49]

Figure 7a and b shows the TEM images of the CNMs grown on CFA and Mag-CFA using pyrolysis oil vapour as the carbon precursor, respectively. Similar to when ethylene gas was used, the CNMs were observed to be anchored on the surface of the cenosphere when CFA was used as catalyst support. As already confirmed by SEM, the quantity of the obtained nanofibers is quite low. The resultant CNMs when Mag-CFA was used were found to be MWCNTs (Figure 7b). The MWCNTs were not of good quality since they had clustered and grown intertwined amongst each other. This suggests that the type of carbon precursor used plays a very important role in determining the type and yield of CNMs.[ 50]

To understand the graphitic nature of the obtained carbon nanomaterial, the samples were analyzed using Raman spectroscopy. Figure 8a and b presents the Raman shift of CNMs

synthesized using coal fly ash and its magnetic fraction using both ethylene and pyrolysis oil vapour, respectively. The Raman spectra for the materials were fitted using the Lorentzian curve fitting (Lorentzians). Both CFA-Cethy and CFA- Cpy have a D band (defective carbon) at 1344 $cm^{-1}$ and G band (graphitic carbon) at 1598 $cm^{-1}$. On the other hand, Mag-Cethy and Mag-Cpy have a D-band at 1348 $cm^{-1}$ and 1341 $cm^{-1}$ and G-band located at 1581 $cm^{-1}$ and 1592 $cm^{-1}$, respectively. The D band emanates from the presence of graphene edges that gives off hybridized vibrational mode illustrating the disarrangement of the graphene structure.[25]

The G band originates from the oscillations that are diverging from the carbon atoms.[25,26,42] If the intensity ratio of G and the D peaks ($I_G/I_D$) is high, it indicates the degree of wall graphitization which gives quality CNTs/CNFs with low defects and high crystallinity. [42,44,54] In this study, the D band peaks of all materials are more prominent except for Mag-Cethy which suggested that the obtained CNMs consist of defects, however more graphitic due to the higher intensity ratios. The $I_G/I_D$ intensity ratios of the CNMs grown on CFA using both ethylene and pyrolysis oil vapour are the same with the value of 1.18, as indicated in Table 2. This suggests that the materials are more graphitic and has minor defects. The graphitization of the materials were also confirmed by XRD peaks at $2\theta=25.5^{o}$ and $2\theta=43^{o}$. The CNMs from magnetic fraction (Mag-Cpy and Mag-Cethy) had intensity ratios of 1.17 and 1.18 respectively. These values are consistent with reports where coal fly ash was used as support for synthesis of CNMs. [42,44] In this case, the authors reported $I_G/I_D$ ratios of 1.35 and 1.4 when acetylene was used for CNMs synthesis at 750 ºC. In that study, the results had indicated that the materials had a high degree of wall graphitization suggesting good quality CNTs. When ethylene was used as carbon precursor at 700 ºC, Dunes et al [54] also reported good quality of CNTs with the intensity ratio of 1.2.

## Conclusions

This study has demonstrated that there is potential for utilization of pyrolysis oil vapour/gas as a carbon precursor in the synthesis of carbon nanofibers/tubes (CNF/Ts). The use of coal fly ash (CFA) and its Fe-rich magnetic fraction (Mag-CFA) also presents an additional advantage for driving down the cost of produced CNF/Ts. The nanocarbons obtained from CFA (when using ethylene gas) showed the growth of both CNFs and CNTs whereas those synthesized using the magnetic fraction had multi-walled carbon nanotubes (MWCNTs). Only MWCNTs were obtained when pyrolysis oil vapour was utilized. Importantly, the type of carbon precursor was found to play an important role in determining the growth mechanism of the resulting nanocarbons.

## Acknowledgements

The authors of this paper would like to thank the South African Department of Science and Technology (DST) for the financial support towards HySA Infrastructure (Grant No. HTC004X), the Council for Scientific and Industrial Research (CSIR) for providing facilities and National Research Foundation (NRF) for funding the SA-Poland collaborative project (HTC071X). Any opinions, findings and/or recommendations expressed in this study are those of the authors and not of the funding bodies.

## References

1. Prasek, J.; Drbohlavova, J.; Chomoucka, J.; Hubalek, J.; Jasek, J. O.; Adam, V.; Kizek, R. Methods for carbon nanotubes synthesis—review. J. Mater. Chem. **2011**, *21* (40), 15872-15884.

2. Eatemadi, A.; Daraee, H.; Karimkhanloo, H.; Kouhi, M.; Zarghami, N.; Akbarzadeh, A.; Joo, S. W. Carbon nanotubes: properties, synthesis, purification, and medical applications. J. Mater. Chem. **2014**, *9* (1), 393-415.

3. Demczyk, B. G.; Wang, Y. M.; Cumings, J.; Hetman, M.; Han, W.; Zettl, A.; Ritchie, R. O. Direct mechanical measurement of the tensile strength and elastic modulus of multiwalled carbon nanotubes. Mater. Sci. Eng. A. **2002**, *334* (1), 173-178.

4. Thostenson, E. T.; Ren, Z.; Chou, T. W. Advances in the science and technology of carbon nanotubes and their composites: a review. Compos. Sci. Technol. **2001**, *61* (13), 1899-1912.

5. Kaushik, B. K; Majumder, M. K. Carbon Nanotube: Properties and Applications. Carbon Nanotube Based VLSI Interconnects,1st Ed.;Springer Briefs in Applied Sciences and Technology, **2015**, DOI 10.1007/978-81-322-2047-3.

6. Dresselhaus, M. S.; Dresselhaus, G.; Jorio, A.; Souza Filho, A. G.; Saito, R. Raman spectroscopy on isolated single wall carbon nanotubes. Carbon. **2002**,*40* (12), 2043-2061.

7. Dresselhaus, M. S.; Dresselhaus, G.; Saito, R.; Jorio, R. A. Raman spectroscopy of carbon nanotubes. Phys. Rep. **2005**, *409* (2), 47-99.

8. Lima, M. D.; Bonadiman, R.; De Andrade, M. J.; Toniolo, J.; Bergmann, C. P. Synthesis of multi-walled carbon nanotubes by catalytic chemical vapor deposition using $Cr_{2-x}Fe_xO_3$ as catalyst. Diamond Relat. Mater. **2006**, *15* (10), 1708-1713.

9. Martin-Gullon, I.; Vera, J.; Conesa, J. A.; González, J. L.; Merino, C. Differences between carbon nanofibers produced using Fe and Ni catalysts in a floating catalyst reactor. Carbon. **2006**, *44* (8), 1572-1580.

*10*. Dervishi, E.; Li, Z.; Xu, Y.; Saini, V.; Biris, A.R; Lupu, D.; Biris, A.S. Carbon nanotubes: synthesis, properties, and applications. Part. Sci. Technol. **2009**, *27* (2), 107–125.

11. Zhou ,W.; Han, Z.; Wang, J.; Zhang, Y.; Jin, Z.; Sun, X.; Li, Y. Copper catalyzing growth of single-walled carbon nanotubes on substrates Nano Lett. **2006**, *6* (12), 2987-2990.

12. Singh, C.; Shaffer, M. S.; Windle, A. H. Production of controlled architectures of aligned carbon nanotubes by an injection chemical vapour deposition method. Carbon. **2003**, *41* (12), 359-368.

13. Wang, S. Application of solid ash based catalysts in heterogeneous catalysis. Environ. Sci. Technol. **2008**, *42* (19), 7055-7063.

14. Magrez, A.; Seo, J. W.; Smajda, R.; Mionić, M.; Forró, L. Catalytic CVD synthesis of carbon nanotubes: towards high yield and low temperature growth. Mater. **2010**, *3* (11), 4871-4891.

15. Suda, Y.; Maruyama, K.; Iida, T.; Takikawa, H.; Ue, H.; Shimizu, K.; Umeda, Y. High-Yield Synthesis of Helical Carbon Nanofibers Using Iron Oxide Fine Powder as a Catalyst. Cryst. **2015**, *5* (1), 47-60.

16. De Jong, K.P.; Geus, J. W. Carbon nanofibers: catalytic synthesis and applications. Cat. Rev. Sci. Eng. **2000**, *42* (4), 481-510.

17. Park, C.; Baker, R.T.K. Carbon deposition on iron–nickel during interaction with ethylene–hydrogen mixtures. J. Catal. **1998**, *179* (2), 361-374.

18. Yu, Z.; Chen, D.; Rønning, M.; Tøtdal, B.; Vrålstad, T.; Ochoa-Fernández, E.; Holmen, A. Large-scale synthesis of carbon nanofibers on Ni-Fe-Al hydrotalcite derived catalysts: II: Effect of Ni/Fe composition on CNF synthesis from ethylene and carbon monoxide. Appl. Catal. A. **2008**, *338* (1),147-158.

19. Carneiro, O. C.; Rodriguez, N.M.;Baker, R.T.K. Growth of carbon nanofibers from the iron–copper catalyzed decomposition of $CO/C_2H_4/H_2$ mixtures. Carbon.**2005**, *43* (11),2389-2396.

20. Gupta, D.K.; Rai, U.N.; Tripathi, R.D.; Inouhe, M. Impacts of fly-ash on soil and plant responses. J. Plant Res. **2002**, *115* (6), 401-409.

21. Jala, S.; Goyal, D. Fly ash as a soil ameliorant for improving crop production—a review. Bioresour. Technol. **2006**, *97* (9),1136-1147.

22. Franus, W.; Wiatros-Motyka, M. M.; Wdowin, M. Coal fly ash as a resource for rare earth elements. Environ. Sci. Pollut. Res. **2015**, *22* (12),9464-9474.

23. Qu, W.; Zhou, Q.; Wang, Y. Z.; Zhang, J.; Lan, W. W.; Wu, Y. H.; Wang, D. Z. Pyrolysis of waste tire on ZSM-5 zeolite with enhanced catalytic activities. Polym. Degrad. Stab. **2006**, *91* (10), 2389-2395.

24. Williams, P.T. Pyrolysis of waste tyres: a review. Waste Manage. **2013**, *33* (8),1714-1728.

25. Hintsho, N.; Shaikjee, A.; Masenda, H.; Naidoo, D.; Billing, D.; Franklyn, P.; Durbach, S. Direct synthesis of carbon nanofibers from South African coal fly ash. Nanoscale Res. Lett. **2014**, *9* (1), 1-11.

26. Yasui, A.; Kamiya, Y.; Sugiyama, S.; Ono, S.; Noda, H.; Ichikawa, Y. Synthesis of carbon nanotubes on fly ashes by chemical vapor deposition processing. IEEJ Trans. Electr. Electron Eng. **2009**, *4* (6),787-789.

27. Yadav, V. K.; Fulekar, M. H. Isolation and Charcterization of Iron Nanoparticles From Coal Fly Ash From Gandhinagar (Gujarat) Thermal Power Plant (A Mechanical Method of Isolation). Int. J. Eng. Res. Technol. (IJERT). **2014**, *3* (6), 471-477.

28. Mahlaba, J. S.; Kearsley, E. P.; Kruger, R. A. Physical, chemical and mineralogical characterisation of hydraulically disposed fine coal ash from SASOL Synfuels. Fuel. **2011**, *90* (7) , 2491-2500.

29. San Miguel, G.; Aguado, J.; Serrano, D. P.; Escola, J. M. Thermal and catalytic conversion of used tyre rubber and its polymeric constituents using Py-GC/MS. Appl. Catal. B. **2006**, *64* (3), 209-219.

30. Sahoo, P. K.; Kim, K.; Powell, M. A.; Equeenuddin, S. M. Recovery of metals and other beneficial products from coal fly ash: a sustainable approach for fly ash management. Int. J. Coal Sci. Technol. **2016**, *3* (3), 267–283.

31. Luhrs, C.C.; Moberg, M.; Maxson, A.; Brewer, L.; Menon, S. IF-$WS_2$/nanostructured carbon hybrids generation and their characterization. Inorg. **2014**, *2* (2), 211-232.

32. Liang, C.; Xia, W.; Soltani-Ahmadi, H.; Schlüter, O.; Fischer, R. A.; Muhler, M. The two-step chemical vapor deposition of Pd (allyl) Cp as an atom-efficient route to synthesize highly dispersed palladium nanoparticles on carbon nanofibers. Chem. Commun. **2005**, *2* , 282-284.

33. Cao, A.; Zhu, H.; Zhang, X.; Li, X.; Ruan, D.; Xu, C.; Wu, D. Hydrogen storage of dense-aligned carbon nanotubes. Chem. Phys. Lett. **2001**, *342* (5), 510-514.

34. Cao, A.; Xu, C.; Liang, J.; Wu, D.; Wei, B. X-ray diffraction characterization on the alignment degree of carbon nanotubes. Chem. Phys. Lett. **2001**, *344* (1), 13-17.

35. Wang, X.; Li, Q.; Pan,; H.; Lin, Y.; Ke, Y.; Sheng, H.; Wu, G. Size-controlled large-diameter and few-walled carbon nanotube catalysts for oxygen reduction. Nanoscale. **2015**, *7* (47), 20290-20298.

36. Sun, Z.; Liu, Z.; Wang, Y.; Han, B.; Du, J.; Zhang, J. Fabrication and characterization of magnetic carbon nanotube composites. J. Mater. Chem. **2005**, *15* (42), 4497-4501.

37. Siddheswaran, R.; Manikandan, D.; Avila, R. E.; Jeyanthi, C. E.; Mangalaraja, R. V. Formation of carbon nanotube forest over spin-coated $Fe_2O_3$ reduced thin-film by chemical vapor deposition. Fuller. Nanotub. Car. N. **2015**, *23* (5), 392-398.

38. Fenelonov, V. B.; Mel'gunov, M.S.; Parmon, V.N. The properties of cenospheres and the mechanism of their formation during high-temperature coal combustion at thermal power plans. KONA Powder Part. J. **2010**, *28* , 189-208.

39. Ahmaruzzaman, M. A review on the utilization of fly ash. Prog. Energy Combust. Sci. **2010**, *36* (3), 327-363.

40. Adeniran, B.; Mokaya, R. Compactivation: a mechanochemical approach to carbons with superior porosity and exceptional performance for hydrogen and $CO_2$ storage. Nano Energy. **2015**, *16* 173-185.

41. Deck, C.P.; Vecchio, K. Prediction of carbon nanotube growth success by the analysis of carbon–catalyst binary phase diagrams. Carbon. **2006**, *44* (2), 267-275.

42. Salah, N.; Al-Ghamdi, A.A.; Memic, A.; Habib, S.S.; Khan, Z. H. Formation of Carbon Nanotubes from Carbon-Rich Fly Ash: Growth Parameters and Mechanism, Mater. Manuf. Processes. **2015**, *31* (2), 146-156.

43. Saleh, T.A.; Danmaliki, G.I. Adsorptive desulfurization of dibenzothiophene from fuels by rubber tyres-derived carbons: Kinetics and isotherms evaluation. Process Saf. Environ. Prot. **2016**, *102*, 9-19.

44. Salah, N.; Habib, S.S.; Khan, Z.H.; Memic, A.; Nahas, M.N. Growth of carbon nanotubes on catalysts obtained from carbon rich fly ash. Dig. J. Nanomater. Biostruct. **2012**,*7* (3), 1279-1288.

45. Gohier, A.; Ewels, C. P.; Minea, T. M.; Djouadi, M. A. Carbon nanotube growth mechanism switches from tip-to base-growth with decreasing catalyst particle size. Carbon. **2008**, *46* (10) , 1331-1338.

46. Yu, L.; Sui, L.; Qin, Y.; Du, F.; Cui, Z. Catalytic synthesis of carbon nanofibers and nanotubes by the pyrolysis of acetylene with iron nanoparticles prepared using a hydrogen-arc plasma method, Mater. Lett. **2009**, *63* (20), 1677-79.

47. Sinnott, S. B.; Andrews, R.; Qian, D.; Rao, A. M.; Mao, Z.; Dickey, E. C.; Derbyshire, F. Model of carbon nanotube growth through chemical vapor deposition. Chem. Phys. Lett. **1999**, *315* (1), 25-30.

48. Kumar, M.; Ando, Y. Chemical vapor deposition of carbon nanotubes: a review on growth mechanism and mass production. J. Nanosci. Nanotechnol. **2010**, *10* (6), 3739-3758.

49. Coville, N. J.; Mhlanga, S. D.; Nxumalo, E. N.; Shaikjee, A. A review of shaped carbon nanomaterials. S. Afri. J. Sci. **2011**,*107* (3-4), 1-15.

50. Plata, D.L.; Meshot, E. R.; Reddy, C. M.; Hart, A. J.; Gschwend, P.M. Multiple alkynes react with ethylene to enhance carbon nanotube synthesis, suggesting a polymerization-like formation mechanism. ACS nano. **2010**, *4* (12), 7185-7192.

51. Ngu, L. N.; Wu, H.; Zhang, D. K. Characterization of ash cenospheres in fly ash from Australian power stations. Energy Fuels. **2007**, *21* (6), 3437-3445.

52. Lai, H. J.; Lin, M. C. C.; Yang, M. H.; Li, A. K. Synthesis of carbon nanotubes using polycyclic aromatic hydrocarbons as carbon sources in an arc discharge. Mater. Sci. Eng. C **2001**, *16* (1), 23–26.

53. Ismagilov, Z. R.; Shalagina, A. E.; Podyacheva, O. Y.; Ischenko, A. V.; Kibis, L. S.; Boronin, A. I.; Buryakov, T. I. Structure and electrical conductivity of nitrogen-doped carbon nanofibers. Carbon. **2009**, *47* (8), 1922-1929.

54. Dunens, O. M.; MacKenzie, K. J.; Harris, A. T. Synthesis of multiwalled carbon nanotubes on fly ash derived catalysts. Environ. Sci. Technol. **2009**, *43,* 7889-7894.

## FIGURES CAPTIONS

**Figure 1**. XRD of the a) CFA and b) Magnetic fraction. M=Mullite, Q=Quartz, Ma=Magnetite, H=Hematite.

**Figure 2**. XRD for a) CNMs grown on CFA using ethylene and b) CNMs grown on CFA using pyrolysis oil vapour.

**Figure 3**. XRD for a) CNMs grown on magnetic fraction using ethylene and b) CNMs grown on magnetic fraction using pyrolysis oil vapour.

**Figure 4.** The SEM images of a) as received coal fly ash b)magnetic fraction from CFA, CNMs grown on CFA using c) ethylene as carbon precursor d) pyrolysis oil as carbon precursor, CNMs grown on magnetic fraction from CFA using e) ethylene and f) pyrolysis oil vapour as carbon precursor.

**Figure 5**. TEM images of CNMs grown using ethylene as carbon precursor a) CNFs anchored on the surface of the cenosphere b) MWCNTs grown from magnetic fraction from CFA c) the metal catalyst situated at the tip of the filament.

**Figure 6**. a) Tip growth mechanism b) CNF herringbone morphology[14].

**Figure 7**. TEM images of CNMs grown using pyrolysis oil vapour as carbon precursor a) CNFs anchored on the surface of the cenosphere b) MWCNTs grown from magnetic fraction of CFA.

**Figure 8**. Raman Spectra of a) CNMs grown on CFA and b) CNMs grown on CFA magnetic fraction using both ethylene and pyrolysis oil vapour.

## TABLES CAPTIONS

**Table 1.** Elemental analysis of the staring materials coal fly ash and its magnetic fraction

**Table 2.** Values of D and G peaks of the Raman spectra including the intensity ratios

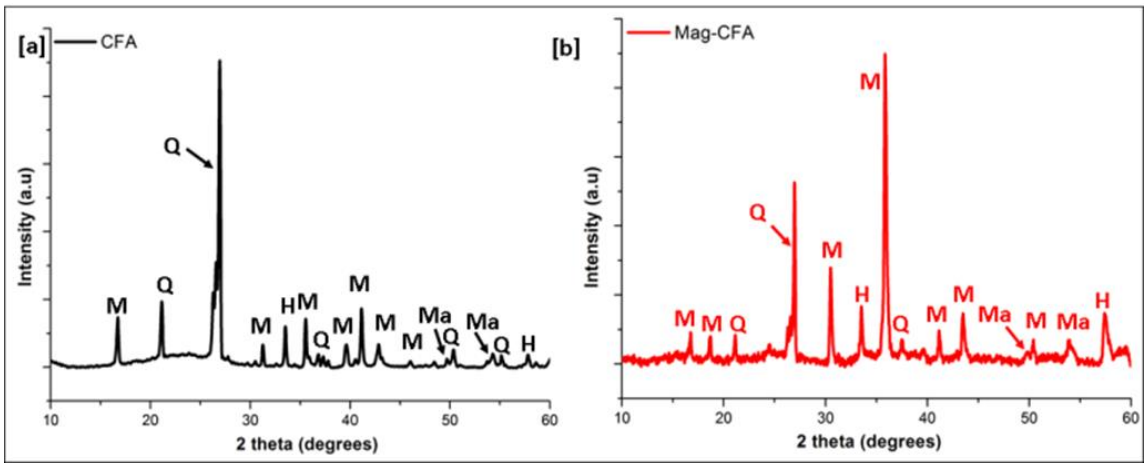


Fig. 1

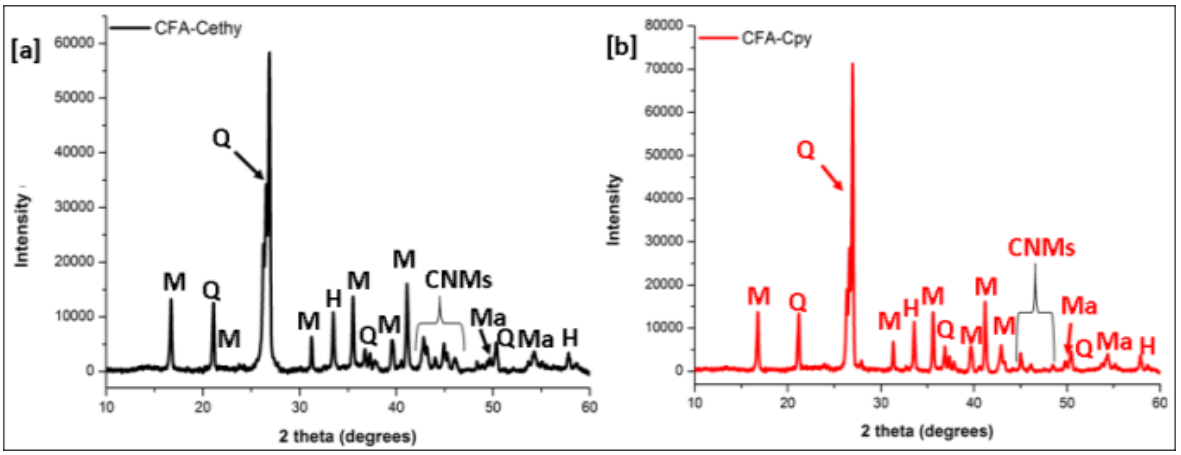
[a]
CFA-Cethy
Intensity
2 theta (degrees)
Q
M
H
CNMs
Ma
[b]
CFA-Cpy
Intensity
2 theta (degrees)
Q
M
H
CNMs
Ma

Fig. 2

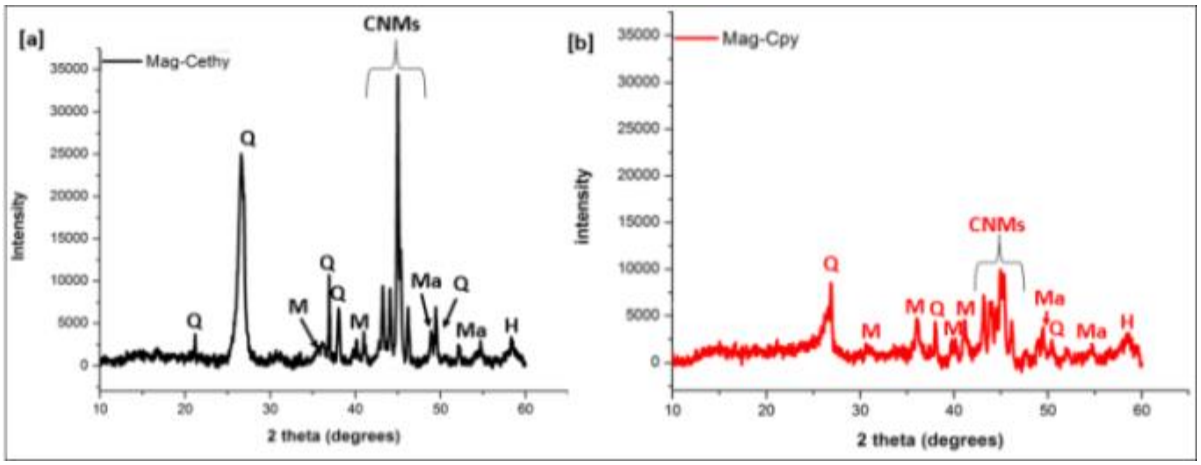
[a]
Mag-Cethy
Intensity
2 theta (degrees)
CNMs
Q
M
Ma
H
[b]
Mag-Cpy
intensity
2 theta (degrees)
CNMs
Q
M
Ma
H

Fig. 3

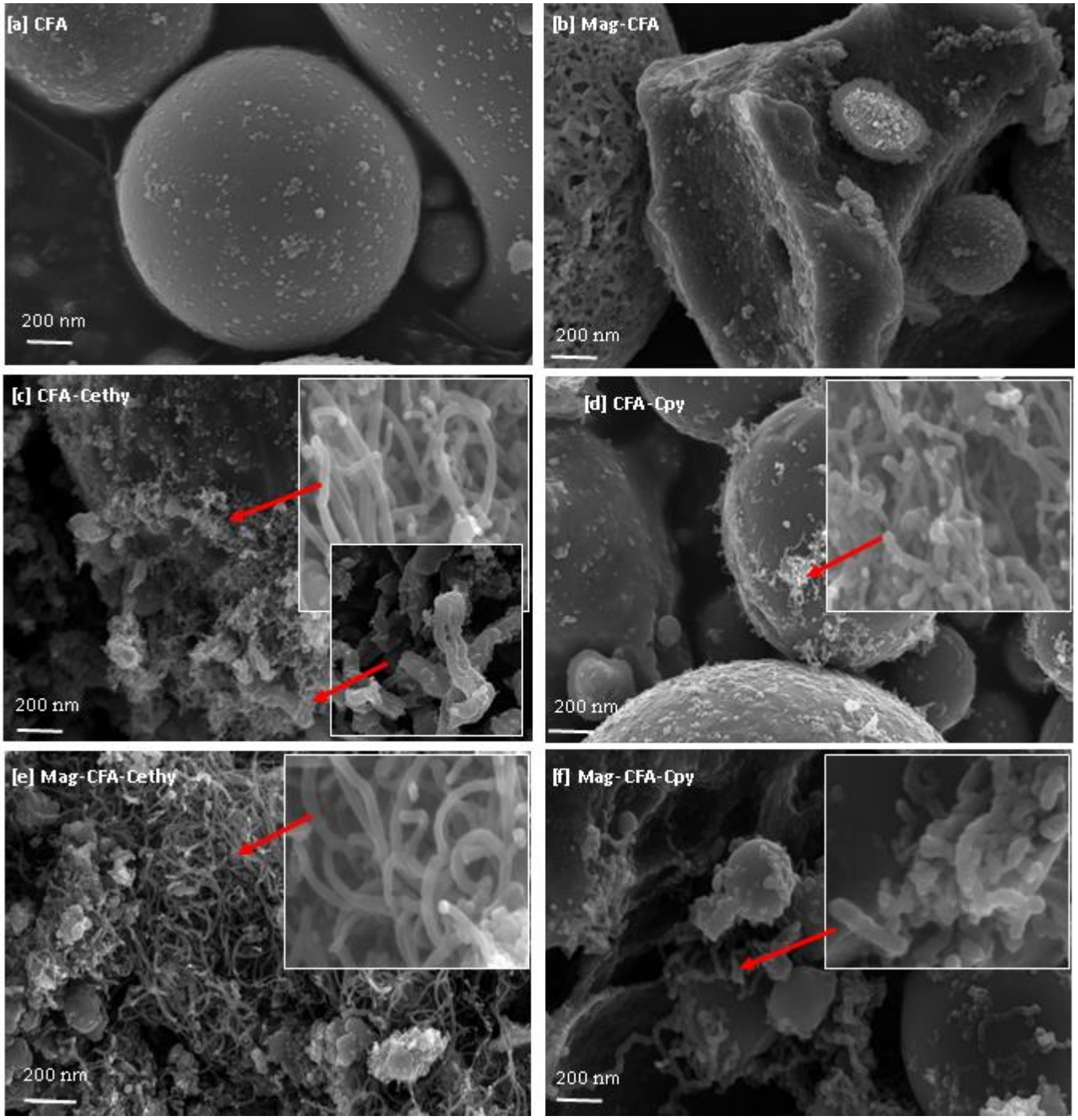
[a] CFA
200 nm
[b] Mag-CFA
200 nm
[c] CFA-Cethy
200 nm
[d] CFA-Cpy
200 nm
[e] Mag-CFA-Cethy
200 nm
[f] Mag-CFA-Cpy
200 nm

Fig. 4

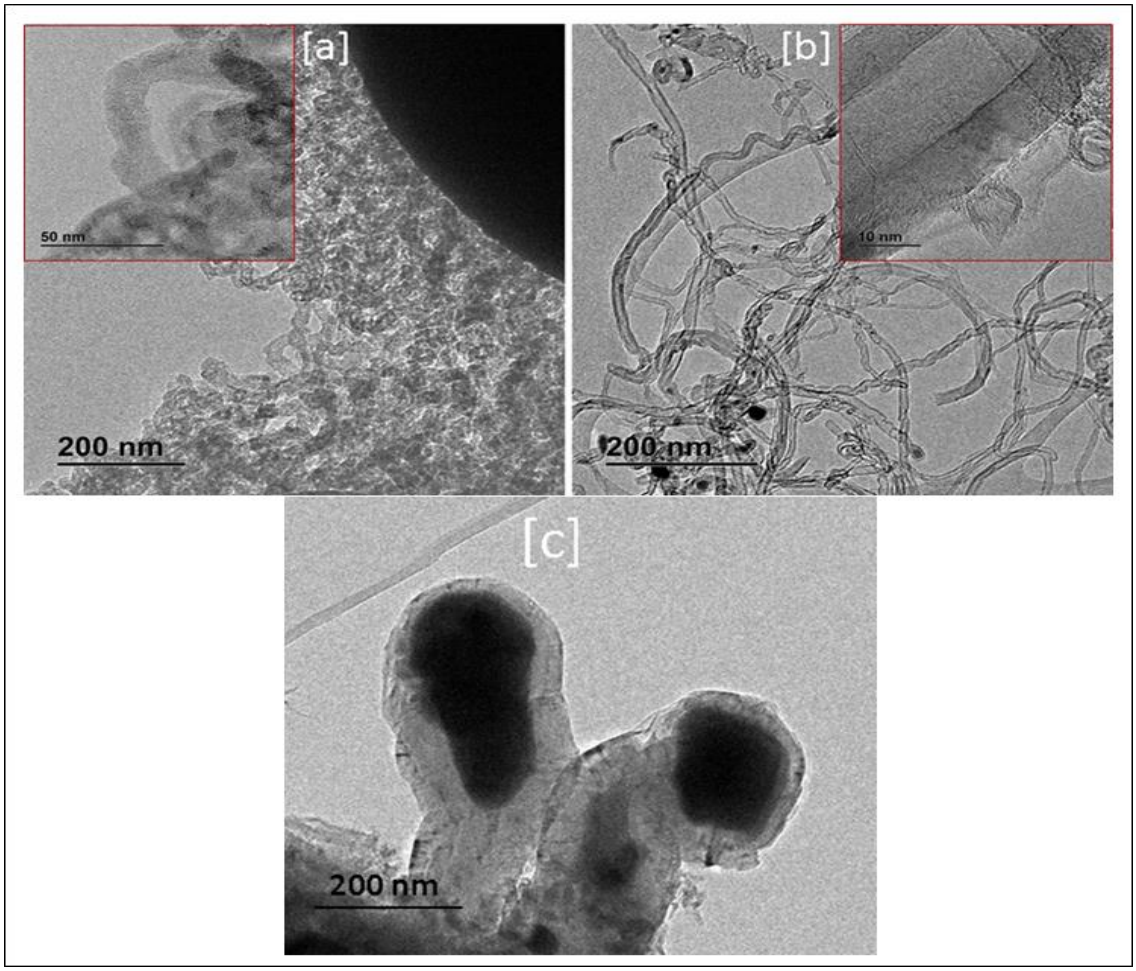
[a]
50 nm
200 nm
[b]
10 nm
200 nm
[c]
200 nm

Fig. 5

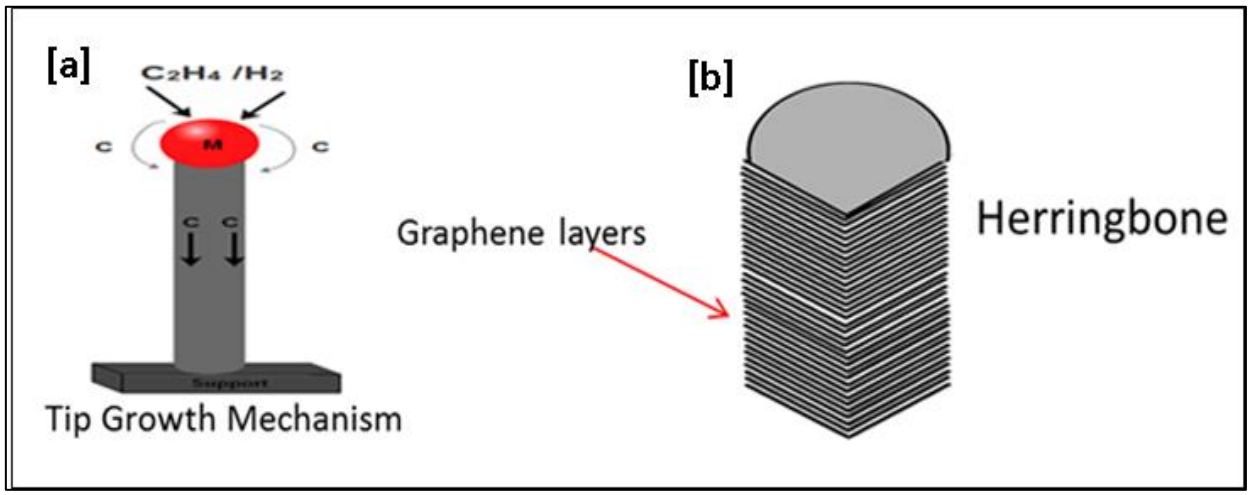
[a]
C2H4 /H2
M
C
C
C
C
Tip Growth Mechanism
[b]
Graphene layers
Herringbone

Fig. 6

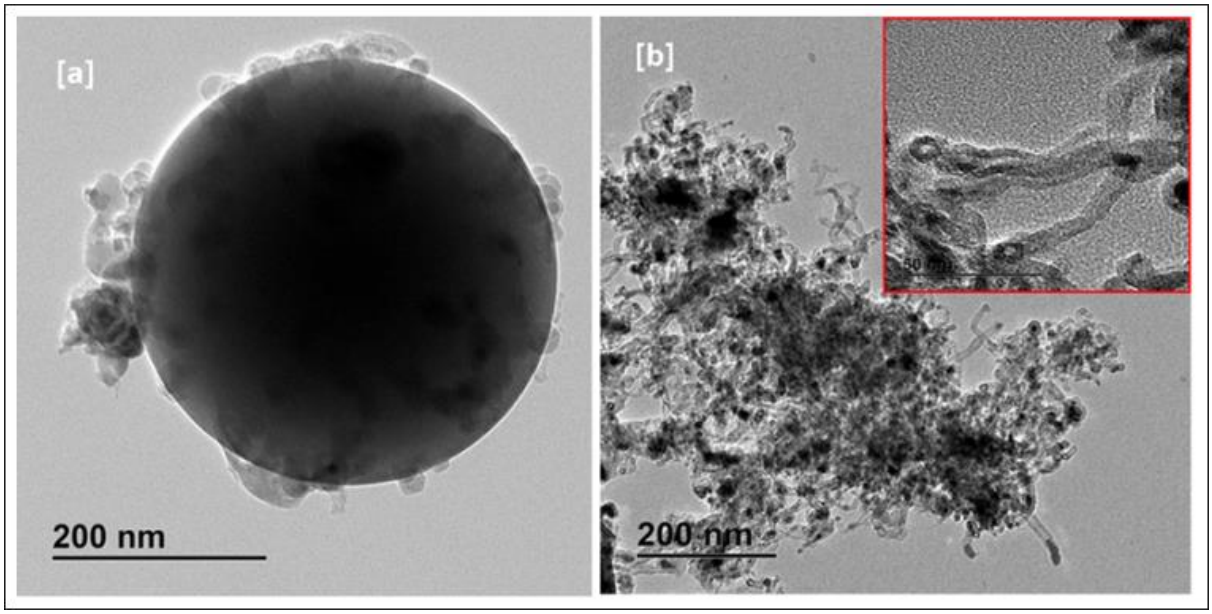
[a]
200 nm
[b]
200 nm

Fig. 7

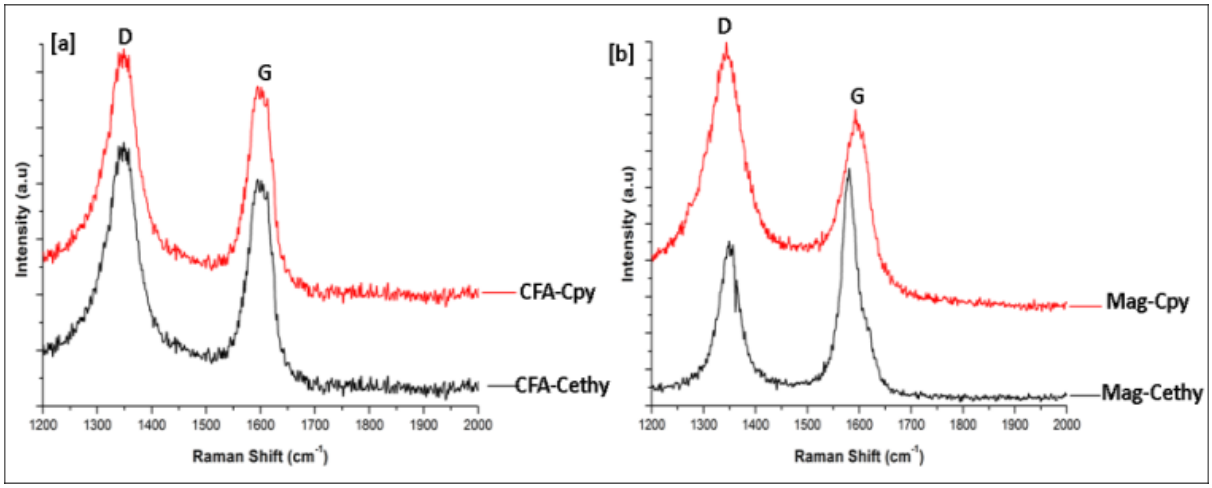
[a]
D
G
Intensity (a.u)
CFA-Cpy
CFA-Cethy
1200 1300 1400 1500 1600 1700 1800 1900 2000
Raman Shift (cm-1)
[b]
D
G
Intensity (a.u)
Mag-Cpy
Mag-Cethy
1200 1300 1400 1500 1600 1700 1800 1900 2000
Raman Shift (cm-1)

Fig. 8

**Table 1.** Elemental analysis of the staring materials coal fly ash and its magnetic fraction

| Elements (wt. %) | Coal | Fly Ash | Magnetic Fraction |
|---|---|---|---|
| **Si** | | 62.45 | 15.07 |
| **Al** | | 26.17 | 11.27 |
| **Fe** | | 3.57 | 66.9 |
| **Ca** | | 3.63 | 4.13 |
| **Ti** | | 2.50 | 1.57 |
| **Mg** | | 0.70 | 0.63 |
| **K** | | 1.00 | 0.47 |

**Table 2.** Values of D and G peaks of the Raman spectra including the intensity ratios

| Sample | D ($cm^{-1}$) | G ($cm^{-1}$) | $I_G/I_D$ |
|---|---|---|---|
| **CFA-Cethy** | 1344 | 1598 | 1.18 |
| **CFA-Cpy** | 1344 | 1598 | 1.18 |
| **Mag-Cethy** | 1348 | 1581 | 1.17 |
| **Mag-Cpy** | 1341 | 1592 | 1.18 |